Quantifying Putative Retinal Gliosis in Preclinical Alzheimer's Disease

Swetha Ravichandran,[1] Peter J. Snyder,[2,3] Jessica Alber,[3–5] Madelyn R. Kenny,[1] Andrew Rothstein,[1] Keisha Brown,[1] Charles F. Murchison,[6,7] Olivio J. Clay,[6,8] Erik D. Roberson,[6] and Edmund Arthur[1]

[1]School of Optometry, University of Alabama at Birmingham, Birmingham, Alabama, United States
[2]Department of Neurology, Alpert Medical School of Brown University, Providence, Rhode Island, United States
[3]Department of Biomedical and Pharmaceutical Sciences, University of Rhode Island, Kingston, Rhode Island, United States
[4]George and Anne Ryan Institute for Neuroscience, University of Rhode Island, Kingston, Rhode Island, United States
[5]Butler Hospital Memory and Aging Program, Providence, Rhode Island, United States
[6]Alzheimer's Disease Research Center, Department of Neurology, University of Alabama at Birmingham, Birmingham, Alabama, United States
[7]Department of Biostatistics, University of Alabama at Birmingham, Birmingham, Alabama, United States
[8]Department of Psychology, University of Alabama at Birmingham, Birmingham, Alabama, United States

Correspondence: Edmund Arthur, School of Optometry, University of Alabama at Birmingham, 1716 University Blvd, Birmingham, AL 35294, USA; earthur@uab.edu.

Received: January 22, 2024
Accepted: April 9, 2024
Published: May 2, 2024

Citation: Ravichandran S, Snyder PJ, Alber J, et al. Quantifying putative retinal gliosis in preclinical Alzheimer's disease. *Invest Ophthalmol Vis Sci.* 2024;65(5):5. https://doi.org/10.1167/iovs.65.5.5

Purpose. Neuroinflammation plays a significant role in the pathology of Alzheimer's disease (AD). Mouse models of AD and postmortem biopsy of patients with AD reveal retinal glial activation comparable to central nervous system immunoreactivity. We hypothesized that the surface area of putative retinal gliosis observed in vivo using en face optical coherence tomography (OCT) imaging will be larger in patients with preclinical AD versus controls.

Methods. The Spectralis II instrument was used to acquire macular centered 20 × 20 and 30 × 25-degrees spectral domain OCT images of 76 participants (132 eyes). A cohort of 22 patients with preclinical AD (40 eyes, mean age = 69 years, range = 60–80 years) and 20 control participants (32 eyes, mean age = 66 years, range = 58–82 years, $P = 0.11$) were included for the assessment of difference in surface area of putative retinal gliosis and retinal nerve fiber layer (RNFL) thickness. The surface area of putative retinal gliosis and RNFL thickness for the nine sectors of the Early Treatment Diabetic Retinopathy Study (ETDRS) map were compared between groups using generalized linear mixed models.

Results. The surface area of putative retinal gliosis was significantly greater in the preclinical AD group (0.97 ± 0.55 mm^2) compared to controls (0.68 ± 0.40 mm^2); $F_{(1, 70)} = 4.41$, $P = 0.039$; Cohen's d = 0.61. There was no significant difference between groups for RNFL thickness in the 9 ETDRS sectors, $P > 0.05$.

Conclusions. Our analysis shows greater putative retinal gliosis in preclinical AD compared to controls. This demonstrates putative retinal gliosis as a potential biomarker for AD-related neuroinflammation.

Keywords: putative retinal gliosis, preclinical Alzheimer's disease (AD), en face spectral domain optical coherence tomography (SD-OCT) imaging, retinal nerve fiber layer (RNFL) thickness, multimodal model

Alzheimer's disease (AD) is a progressive neurodegenerative disease that ranks as the most common cause of dementia in the elderly accounting for about 60% to 80% of all cases.[1] Pathological changes in AD precede any symptomatic changes by almost 2 decades.[2–7] The progression of the disease referred to as the AD continuum signifies the transition from pathological changes in the brain that are unobtrusive to the individual to those changes that cause memory problems and disability.[8,9] The initial stage of the continuum, the preclinical phase, is the period where the individual exhibits no symptomatic changes but shows measurable biomarker abnormality like amyloid beta (Aβ) deposition, as measured using brain positron emission tomography (PET) scans or cerebrospinal fluid (CSF) assessment via lumbar puncture.[10,11] The preclinical stage is typically followed by mild cognitive impairment (MCI) due to AD and subsequently by dementia due to AD. The goal is to detect the disease during the preclinical phase when emerging therapeutics are likely to be most effective. PET and CSF assessment have not been widely used in clinical practice because they are expensive and invasive, respectively. Although blood-based biomarkers have greater likelihood of becoming part of the normal clinical diagnostic pathway within the next

few years,[12–14] there is still a need for other noninvasive biomarkers.

As an extension of the brain,[15,16] the retina provides a potential noninvasive window for early diagnosis of AD.[17–23] Neuroinflammation is a common pathological feature in AD.[24,25] Mouse models of AD and postmortem biopsy of patients with AD reveal retinal glial activation comparable to the central nervous system (CNS) immunoreactivity.[26–28] The neurosensory retina houses glial cells, including Müller cells, astrocytes, and microglia. Müller cells are radial cells that span the entire retina. Astrocytes are predominantly found in the retinal nerve fiber layer (RNFL), and microglia reside predominantly in the inner plexiform and outer plexiform layers (IPL and OPL), but they are also present in small proportion in the retinal ganglion cell (RGC) layer, RNFL, and at the internal limiting membrane (ILM) junction.[29,30]

The classical structural biomarker investigated in AD with respect to the neurosensory retina includes the RNFL thickness at the macular (mRNFL) and the peripapillary region (pRNFL). Investigations into RNFL thickness during the preclinical and MCI stages of AD yield conflicting results.[21,31–34] Quadrant-specific RNFL thinning in patients with MCI due to AD has been shown but the region of the RNFL affected varies substantially between studies.[35,36] In contrast, other studies did not find significant differences in RNFL thickness between MCI and cognitively unimpaired (CU) participants altogether.[37,38] Nonsignificant results in RNFL thickness have also been found in preclinical AD.[32–34] Interestingly, thicker mRNFL has been reported in participants with MCI due to AD compared with AD dementia and CU participants, with the areas of thickening hypothesized to be a result of neuroinflammation or gliosis in the RNFL bundle.[21,31] This can be explained by the fact that the hyper-reflective band of the RNFL on spectral domain optical coherence tomography (SD-OCT) is made up of not only RNFL bundles, but also contains non-neural components including retinal glial cells (astrocytes, microglia, and end feet of Müller cells) and blood vessels.[39–43] When there is thinning of the RNFL hyper-reflective band shown on SD-OCT in AD,[18–20,22,23,35,36] it is assumed that the atrophy of the RNFL bundles is what drives the reduction of the RNFL thickness. However, this thinning could be due to atrophy of the non-neural structures in the RNFL hyper-reflective band. In addition, variability in blood vessel diameter, activated microglia, and astrocytes (gliosis) in the RNFL hyper-reflective band may also cause artifacts in thickness measurements[44–46] and thereby account for studies that report thinning/thickening/null results of the RNFL in MCI[21,31,35–38] or nonsignificant results in RNFL thickness in preclinical AD.[32–34] All the above results point to lack of consistency in RNFL thickness measure to be used as a unique biomarker for AD.

SD-OCT en face images of individual retinal layers can be generated from dense or volume scans by using information segmented from specific retinal layers.[44–47] Putative retinal gliosis (activated retinal astrocytes, microglia, and Müller cells) has been quantitatively characterized as hyper-reflective patches on SD-OCT en face images that correspond to similar structures on the b-scans in glaucoma,[45,48–50] diabetic retinopathy,[51–53] and retinal vein occlusion.[54] The presence of these hyper-reflective structures (putative gliotic changes) and the extent of retinal region covered with them have been reported to have a greater potential of being an indicator for glaucomatous degeneration.[45] These areas of putative gliosis are also increased in proliferative diabetic retinopathy compared to nonproliferative and control participants, with patients with diabetic macular edema having larger areas compared to patients with no macular edema.[53]

The goal of the current study was three-fold: (1) investigate differences in the surface area of putative retinal gliosis in vivo using SD-OCT en face imaging in preclinical AD versus controls, (2) examine association between the surface area of putative retinal gliosis versus RNFL thickness, and (3) determine whether a multimodal model of the surface area of putative retinal gliosis and RNFL thickness would better distinguish between preclinical AD and controls compared to a model of the surface area of putative retinal gliosis alone.

Methods

Study Participants

This is a cross-sectional multisite study involving 42 participants from the Butler Hospital Memory and Aging Program, Providence, RI (part of the Atlas of Retinal Imaging in Alzheimer's Study; ARIAS) and 51 participants from the University of Alabama at Birmingham (UAB) Alzheimer's Disease Research Center (ADRC). The study protocol adhered to the tenets of the Declaration of Helsinki and was approved by the BayCare and UAB Institutional Review Boards. Written informed consent was obtained from all participants prior to experimental data collection. The inclusion criteria for participants in the study were as follows: age $\geq$ 55 years, absence of or controlled hypertension ($<$ 140/90; Table 1), hyperlipidemia, and systemic diabetes (HbA1c $\leq$ 7; see Table 1). Eyes were excluded if there were any associated retinal pathology that could predispose the individual to developing glial changes like in glaucoma, diabetic retinopathy, retinal ischemic conditions, epiretinal membrane (ERM), age-related macular degeneration, macular hole, other retinal procedures, including pars plana vitrectomy, laser photocoagulation, ILM peeling, etc. Other exclusion criteria included unstable doses of antidepressants that have significant anticholinergic side effects, large cataracts that would impede imaging, current intake of

Table 1. Demographics of the Study Participants

Variables	Control ($N = 20$)	Preclinical AD ($N = 22$)	*P* Value
Age, y (mean ± SD)	66 ± 6	69 ± 5	0.11*
Sex, *n* (%)			0.90†
Male	6 (30)	7 (31.8)	
Female	14 (70)	15 (68.2)	
Race, n (%)			0.57†
Caucasian	18 (90)	21 (95.5)	
Black or African American	1 (5)	—	
Others	1 (5)	1 (4.5)	
Diabetic status, *n* (%)			0.087†
Absent	20 (100)	19 (86.4)	
Controlled (HbA1c $\leq$ 7)	—	3 (13.6)	
Hypertension status, *n* (%)			0.28†
Absent	15 (75)	13 (59.1)	
Controlled (BP $<$ 140/90)	5 (25)	9 (40.9)	

BP, blood pressure.
* Independent samples *t*-test.
† Chi-square test of independence.

retino toxic drugs such as chloroquine, hydroxychloroquine, and cancer drugs, and other neurodegenerative diseases, such as Parkinson's disease or multiple sclerosis. All the eyes involved in the study had best corrected visual acuity ≥ 20/40 (approximately Log MAR = 0.30) and refractive errors ≤ ± 3.00 DS (spherical equivalent) which will correspond to an approximate equivalent axial length of 22 to 24 mm to prevent significant differences in retinal magnification, as noted by the Bennett formula.[55]

Out of the 42 participants from Butler Hospital Memory and Aging Program, 5 participants were excluded due to the presence of image artifacts, ERM, or sheen, and out of the 51 participants from the UAB ADRC, 12 participants were excluded due to presence of ERM, sheen, hypertensive/diabetic retinopathy, and peripheral exudates/heme. Thus, a total of 76 participants (132 eyes) comprising 59 CU older adults, 11 patients with MCI, and 6 patients with Alzheimer's dementia were involved in the study. Out of the 59 CU older adults, 42 participants had Aβ PET results available. A cohort of 22 preclinical AD (7 men and 15 women, 40 eyes, mean age = 69 years, range = 60-80 years; see Table 1) and 20 control participants (6 men and 14 women, 32 eyes, mean age = 66 years, range = 58-82 years; see Table 1; N = 72 eyes) were included for the assessment of difference in surface area of putative retinal gliosis and RNFL thickness. There were no significant differences between the two groups in age (t(40) = 1.65, P = 0.11) or sex (χ^2 (1, N = 42) = 0.016, P = 0.90; see Table 1). Both preclinical AD and control participants were CU based on neuropsychological evaluation. Preclinical AD participants were Aβ PET positive, whereas controls were Aβ PET negative. CU participants had Montreal Cognitive Assessment (MoCA) scores of ≥ 26,[56,57] a Clinical Dementia Rating (CDR) global score of 0[58] (Butler Hospital and UAB ADRC), and Repeatable Battery for the Assessment of Neuropsychological Status Update (RBANS-U) Delayed Memory Index (DMI) scores of ≥ 85[59,60] (Butler Hospital cohort only).

An estimated sample size (N = 52) was computed with the GPower version 3.1 calculator[61] using parameters obtained from a previous study that examined differences in the number of retinal inclusion bodies and thickness of retinal neuronal layers between groups with high versus low neocortical Aβ load[34] (effect size; Cohen's d of 0.80, two-sided α of 0.05, and a power of 0.80). Considering 72 eyes were involved in this study, our study was adequately powered to detect differences in the surface area of putative retinal gliosis and RNFL thickness.

Cognitive Assessment

Syndromal/clinical staging of the Alzheimer's continuum was assessed for the participants from the Butler Hospital Memory and Aging program using MoCA,[56,57] CDR,[58] and RBANS-U,[59,60] whereas participants from the UAB ADRC were classified based on MoCA and CDR. In both scenarios, final clinical staging was done by a trained neuropsychologist or cognitive neuroscientist.

MoCA is a validated highly sensitive tool for early detection of MCI.[56,57] It is a one-page test totaling 30 points that can be administered in approximately 10 minutes. It assesses various domains of cognition involving attention and concentration, executive functions, memory, language, visuospatial skills, orientation, calculations, and conceptual thinking. A score of greater than or equal to 26 classifies the individual as CU.

CDR is a 5-point scale that is widely used to assess the severity of dementia in an individual.[58] Based on observations and interviews with both the patient and an informant, the CDR rates a person's cognitive and functional performance across six domains, including memory, orientation, judgment and problem-solving, community affairs, home and hobbies, and personal care. The 5 levels of the global scores are as follows: CDR 0 – no impairment; CDR 0.5 – questionable cognitive impairment; CDR 1 – mild impairment; CDR 2 – moderate impairment; and CDR 3 – severe impairment.

The RBANS-U is a brief neuropsychological assessment battery that can be administered to adult patients aged 20 to 89 years old.[59,60] The RBANS consists of 10 subtests, which give 5 scores (one for each of 5 domains tested), including immediate memory, visuoperceptual abilities, language, attention, and delayed memory. The RBANS-U DMI score ≥ 85 is considered normal for episodic memory.

Aβ PET Acquisition

To evaluate the level of neocortical amyloid accumulation, each participant underwent an Aβ PET scan. This involved an intravenous injection of 18F-florbetapir at a dose of 370 MBq (10 mCi +/− 10%; Butler Hospital) or C11-PIB (UAB ADRC). Around 50 minutes after the injection, a 20-minute PET scan was conducted along with a head computed tomography (CT) scan to correct for attenuation. The images were captured using a 128 × 128 matrix and then reconstructed using iterative or row action maximization likelihood algorithms. The PET standardized uptake value (SUV) data were summed and standardized against the SUV of the entire cerebellum, creating a ratio known as SUV ratio (SUVr). An SUVr threshold of ≥ 1.1 was considered as Aβ-positive where as an SUVr threshold < 1.1 was considered as Aβ negative, as done previously.[34] These SUVr computations used the MIMneuro software and Aβ positivity/negativity was confirmed in all cases through a read by a board-certified radiologist, respectively, from the Bulter Hospital Memory and Aging Program, Providence, RI, and the UAB ADRC.

SD-OCT Volume Scan Image Acquisition

All participants were dilated with two drops of tropicamide (Mydriacyl 1%) per eye, prior to imaging. Following a 15-minute wait time, dense macular centered 20 × 20 degrees (approximately 6 × 6 mm) SD-OCT images consisting of 512 b-scans, 512 A-scans per b-scan, 12 microns spacing between the b-scans, and 5 frames averaged per each b-scan location was acquired for both eyes of the participants using the Spectralis HRA + OCT (Eye Explorer version 1.10.4.0; Heidelberg Engineering, Heidelberg, Germany). The signal quality values were ensured to be at least 30 to maintain good image quality.

Gliosis Definition and Computation

Reflectance en face images are those that are produced from reflection as a variation of intensity across the underlying anatomy.[62] Putative retinal gliosis characterized by increased reflectivity appeared as white or hyper-reflective patchy structures at the ILM/RNFL boundary en face images (macrophage like cell [MLC layer]; Fig. 1A).[51–54,63] These hyper-reflective patches on the ILM/RNFL boundary en

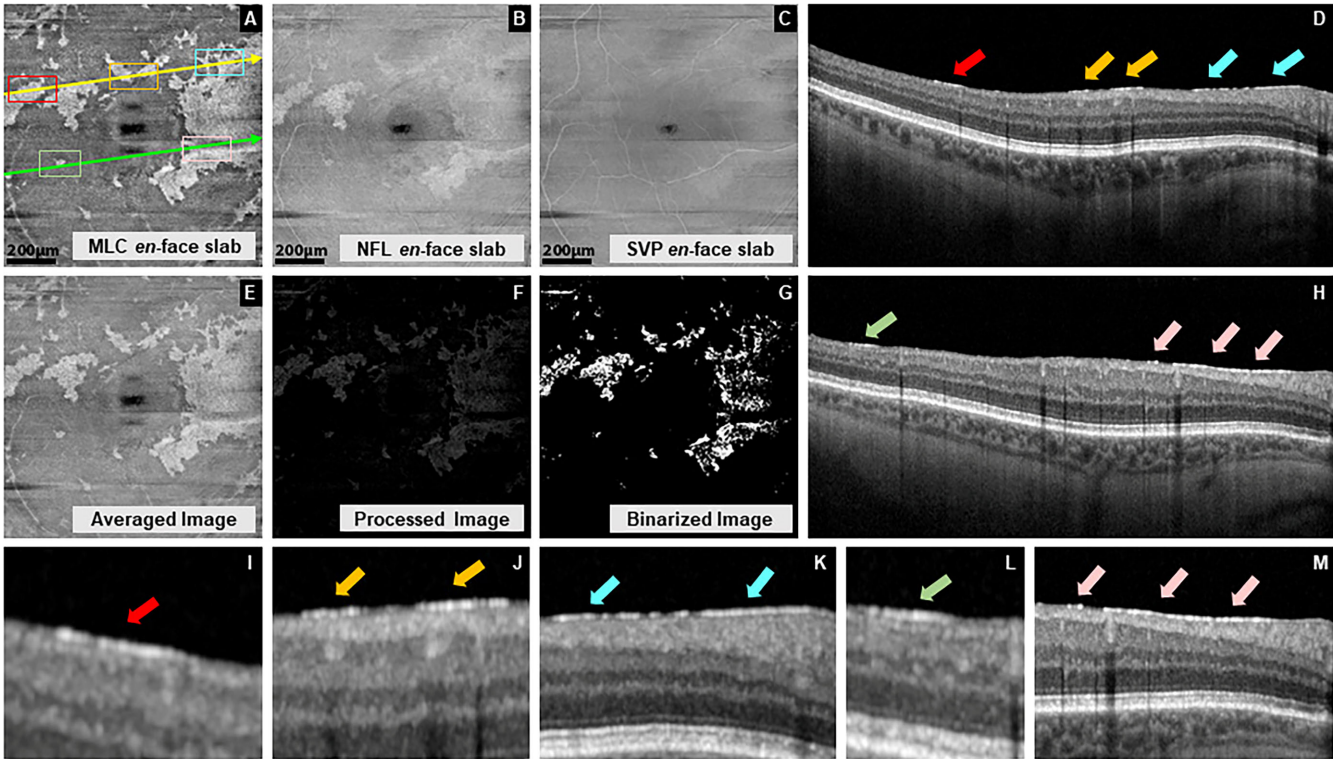

Figure 1. Putative retinal gliosis computation in MATLAB performed using 3 en face slabs in a 60-year-old female patient with preclinical AD with Aβ PET SUVr of 1.53 with no visible posterior vitreous detachment. Three en face slabs were involved in the computation: macrophage like cell (MLC) layer – segmented at the ILM at the vitreoretinal interface (**A**); nerve fiber layer (NFL) – segmented from the ILM to RNFL/RGC layer boundary (**B**) and superficial vascular plexus (SVP) – segmented from the ILM to the IPL/INL boundary (**C**). Averaged MLC and NFL slab (**E**). Sharpened and spatially filtered image after the SVP en face slab has been subtracted from the averaged image to eliminate vascular artifacts (**F**), and binarized image (**G**) for quantification of the surface area of putative retinal gliosis. *White pixels* represent putative retinal gliosis. OCT b-scans corresponding to the cross-sectional location of the *yellow line* (**D**) and the *green line* (**H**) on (**A**). Hyper-reflective patches representing gliosis on en face MLC slab (*red*, *yellow*, *blue*, *green*, and *pink* boxes) displaying similarly color-coded aligned regions of hyper-reflective lines (*red*, *yellow*, *blue*, *green*, and *pink* arrows) on OCT b-scans (**D, H, I–M**).

face images typically corresponded to regions of hyper-reflective lines at the same location on OCT b-scans (see Figs. 1A, 1D, 1H–1M) as reported in other studies.[51–54,63] Other regions of hyper-reflectivity causing artifacts like retinal sheen as a result of specular reflection[45] displayed a bleached appearance and did not correspond to similar locations of hyper-reflectivity lines on the OCT b-scans (Fig. 2). To prevent bias in putative retinal gliosis computation, eyes with artifactual reflectivity were excluded from the analysis.

Computation of putative retinal gliosis was performed using three en face slabs representing: (a) the MLC layer – segmented at the ILM at the vitreoretinal interface[51–54,63] (see Fig. 1A); (b) the NFL – segmented from the ILM to RNFL/RGC layer boundary (see Fig. 1B); and (c) the superficial vascular plexus (SVP) layer – segmented from the ILM to the IPL/inner nuclear layer (INL) boundary (see Fig. 1C).[17] These three en face slabs were obtained from the dense volume SD-OCT scans using the vendor software. The MLC layer en face image has previously been defined via adaptive optics OCT (AO-OCT) imaging as having the highest density of glial structures.[64] Histological and in vivo imaging also show that the RNFL contain non-neural components, such as glial cells and blood vessels.[29,30,39–43] These three SD-OCT en face slabs were automatically cropped to exclude the infrared component and exported into a custom programming software (MATLAB, Mathworks) as .tiff files.

To accurately quantify putative macrophage cells, present at both the ILM interface and the RNFL boundary, the MLC and NFL en face slabs were averaged (see Fig. 1E). The SVP en face slab was then subtracted from the averaged image to eliminate the background and vascular artifacts, thereby preventing unwanted hyper-reflectivity in gliosis computation. Variability in blood vessel diameter/vascular artifacts are known to influence RNFL thickness measurements[44–46] and hence were removed from the computation of putative retinal gliosis. Following this, the image was converted into gray scale for further processing and analysis. Processing of the image involved sharpening and spatial filtering (using a spatial filter of size 3) which was performed to denoise and enhance the area of gliosis in the images (see Fig. 1F).[65] Final analysis involved the binarization process in which pixels above the threshold was converted into white and those below were converted into black pixels (see Fig. 1G). A total count of the white pixels that represent gliosis hyper-reflectivity was obtained. The surface area of putative retinal gliosis was calculated by converting the total number of white pixels into mm^2 based on the micron-to-pixel ratio in the x and y directions, as obtained from the fiducial marks of the vendor software. Data from both eyes were analyzed so far as they were of good image quality and met the inclusion criteria. In cases where only one eye had good image signal quality/met the inclusion criteria, only that eye was selected.

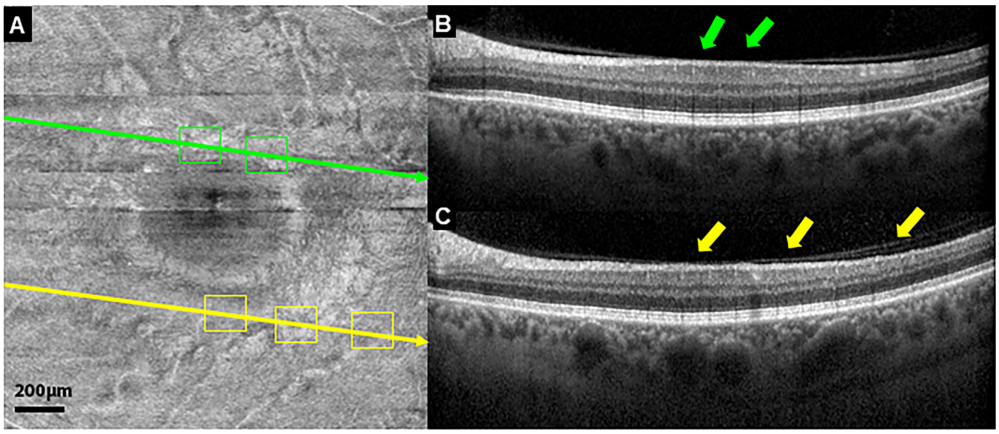

FIGURE 2. Retinal sheen displaying hyperreflectivity on macrophage like cell (MLC) layer en face slab (**A**) and OCT b-scans corresponding to cross sectional location of the *green line* (**B**) and the *yellow line* (**C**) in a 58-year-old CU male participant with Aβ PET SUVr of 0.98. Areas of hyper-reflectivity representing sheen (*green* and *yellow* boxes) on the en face MLC slab (**A**) does not correspond to aligned regions of hyper-reflective lines (*green* and *yellow arrows*; **B** and **C**) on OCT b-scans. MLC slabs with retinal sheen (artifactual hyper-reflectivity) were excluded to prevent bias in putative retinal gliosis computation.

Macular Centered RNFL Thickness

Macular centered SD-OCT images of size 30 × 25 degrees (approximately 8.8 × 7.4 mm) with 61 b-scans, 123 microns spacing between b-scans, and 10 frames averaged per each b-scan location were taken with the Heidelberg Spectralis OCT.[66] The inbuilt Spectralis segmentation software was used to segment the RNFL, as has been done previously.[47] Manual correction of the segmentation of the retinal layers and centration of the Early Treatment Diabetic Retinopathy Study (ETDRS) map[67] was also performed in cases where necessary. The retinal layer segmentation algorithm of the Spectralis has been validated previously.[68] The average RNFL thickness in each of the nine sectoral regions of the ETDRS map[67] was computed using the vendor automated software.

Reliability Assessment for the Computation of Putative Retinal Gliosis and an Example of a Longitudinal Change

To investigate the test-retest reliability for the computation of putative retinal gliosis, a second intra-session image was acquired for participants approximately 2 minutes after the first OCT image acquisition. The test-retest reliability was assessed for the 39 participants (65 eyes) from the UAB ADRC because those were the individuals from whom 2 intra-session images were obtained. Out of the 39 participants from the UAB ADRC, 15 participants had Aβ PET results available of which 5 were CU, 7 were MCI, and 3 had dementia. We therefore included all 39 participants based on clinical/syndromal staging (22 CU participants, 11 patients with MCI, and 6 patients with dementia) to increase the sample size for the test-retest reliability assessment. We also provided a case-in-point example of a 66-year-old female preclinical AD participant with an SUVr of 1.45 to show longitudinal changes in putative retinal gliosis.

Statistical Analyses

Statistical analyses were performed using IBM SPSS Statistics for Windows, version 29 (IBM Corp., Armonk, NY, USA) and R version 4.3.1 software (R Foundation for Statistical Computing, Vienna, Austria). The R statistical software was also used for data visualization purposes using the ggplot2 package. All values are descriptively represented as mean ± SD. Considering a sample size of 72 eyes with kurtosis and skewness of ≤ ± 3.50 for all our outcome variables, normality was assumed, and parametric tests were performed for the data analyses. An independent sample *t*-test was used to compare the difference in age between the groups. Because age was not significant between groups, it was not included as a covariate in our analysis. Considering the binocular eye measurements for the same subject in our study, generalized linear mixed-effects models (GLMMs) were used to assess the difference between preclinical AD and controls where the group served as a fixed effect, participants served as random effects, and the eyes served as the within-subject factor. Individual GLMMs were used to compare the difference in the surface area of putative retinal gliosis and RNFL thickness at the nine ETDRS sectors between groups, accounting for correlation between eyes (Table 2). A P value < 0.05 was considered significant and Cohen's d was used as the effect size measure. An intercept-only mixed-model blocking on OCT region (which nests regions within subjects) was performed to assess association between the surface area of putative retinal gliosis and RNFL thickness across all regions (global RNFL thickness, evaluating the ETDRS regions as a 9-level factor rather than 9 individual models). From there, association between the surface area of putative retinal gliosis and RNFL thickness at the individual ETDRS sectors were examined using Pearson correlation coefficient (Table 3). A mixed-model variation of the single Pearson correlations in Table 3 was also performed to account for the eye as a within-subject factor (Table 4). Absolute agreement, 2-way random-effects model on the k-rater average intraclass correlation coefficient (ICC; value > 0.75 considered acceptable)[69] with 95% confidence interval (CI) was also performed to evaluate the test-retest reliability of the intra-session gliosis measurements for all the 39 participants from the UAB ADRC and then separately for the 22 CU participants (35 eyes) from the same cohort. This was done to show that gliosis measurements were repeatable independent of clinical AD staging (test-retest reliability analysis for the 22 CU participants is analogous to the main 42 partici-

Table 2. Macular Retinal Nerve Fiber Layer (mRNFL) Thickness for the Nine Early Treatment Diabetic Retinopathy Study (ETDRS) Sectors Compared Between Preclinical Alzheimer's Disease and Control Older Adults

Variables	Control (32 Eyes; Mean ± SD)	Preclinical AD (40 Eyes; Mean ± SD)	GLMM Corrected *P* Value
Central RNFL thickness	11.7 ± 2.13 µm	12.5 ± 2.62 µm	0.275
Inner nasal RNFL thickness	20.1 ± 1.91 µm	21.4 ± 3.59 µm	0.161
Outer nasal RNFL thickness	48.4 ± 7.58 µm	49.7 ± 9.79 µm	0.611
Inner superior RNFL thickness	23.1 ± 2.90 µm	24.6 ± 4.24 µm	0.155
Outer superior RNFL thickness	37.4 ± 6.52 µm	38.1 ± 6.76 µm	0.792
Inner temporal RNFL thickness	17.6 ± 1.39 µm	17.6 ± 1.57 µm	0.817
Outer temporal RNFL thickness	19.5 ± 1.76 µm	20.1 ± 1.89 µm	0.213
Inner inferior RNFL thickness	24.1 ± 3.10 µm	25.7 ± 3.65 µm	0.139
Outer inferior RNFL thickness	38.8 ± 6.20 µm	40.5 ± 9.39 µm	0.374

Generalized linear mixed models (GLMMs) were performed to compare mean RNFL thickness between groups, accounting for correlation between eyes.

Table 3. Correlation Between the Surface Area of Putative Retinal Gliosis and the Nine Early Treatment Diabetic Retinopathy Study (ETDRS) Sectors Macular RNFL Thickness

Regions	Pearson Correlation Coefficient	*P* Value
Central RNFL thickness	−0.020	0.87
Inner nasal RNFL thickness	0.318	0.007
Outer nasal RNFL thickness	0.275	0.019
Inner superior RNFL thickness	0.390	<0.001
Outer superior RNFL thickness	0.276	0.019
Inner temporal RNFL thickness	0.191	0.107
Outer temporal RNFL thickness	0.338	0.004
Inner inferior RNFL thickness	0.323	0.006
Outer inferior RNFL thickness	0.228	0.054

Table 4. A Mixed-Model Variation of the Single Pearson Correlations Between the Surface Area of Putative Retinal Gliosis and the Nine Early Treatment Diabetic Retinopathy Study (ETDRS) Sectors Macular RNFL Thickness, Accounting for the Eye as a Within-Subject Factor

Regions	Beta Coefficient	*T*-TEST STATISTIC	*P* Value
Central RNFL thickness	−0.111	−0.255	0.80
Inner nasal RNFL thickness	1.021	1.91	0.063
Outer nasal RNFL thickness	3.22	2.01	0.051
Inner superior RNFL thickness	2.55	3.46	0.001
Outer superior RNFL thickness	2.26	1.91	0.064
Inner temporal RNFL thickness	0.338	1.01	0.317
Outer temporal RNFL thickness	1.08	2.90	0.006
Inner inferior RNFL thickness	1.84	2.43	0.02
Outer inferior RNFL thickness	2.05	1.47	0.148

pants in our study). A Bland-Altman plot was used to evaluate the 95% limits of agreement between the 2 intra-session putative retinal gliosis measurements for the 39 participants from the UAB ADRC. A linear regression of the differences between the two sessions versus the average tested whether there was a proportional bias in the Bland-Altman plot.[70] An initial logistic regression model was created to obtain predictive probabilities for preclinical AD based on gliosis measurements only. A second logistic regression model was created using a combination of gliosis, inner inferior, inner superior, and inner nasal RNFL thicknesses to obtain predictive probabilities. The inner inferior, inner superior, and inner nasal RNFL thicknesses were chosen for the second model since they were close to significance when compared between the groups (see Table 2). A receiver operating characteristic (ROC) curve was constructed in both logistic regression models to assess the sensitivity, specificity, and area under the curve (AUC) to distinguish between the two regression designs. The maximum Youden's index was chosen to establish cutoffs (see Supplementary Fig. S1). The following AUC categorization was used for the study: 0.5 to 0.6 = unsatisfactory, 0.6 to 0.7 = satisfactory, 0.7 to 0.8 = good, 0.8 to 0.9 = very good, and 0.9 to 1 = excellent.

Results

Test-Retest Reliability Analysis for Putative Retinal Gliosis

We first assessed test-retest reliability for the putative retinal gliosis measurement by analyzing 2 separate intra-session images from 39 participants from the UAB ADRC. Test-retest reliability of the surface area of putative retinal gliosis was good, ICC = 0.88 (95% CI = 0.81-0.93), $P < 0.001$ for all 39 participants from the UAB ADRC, and excellent, ICC = 0.93 (95% CI = 0.86-0.96), $P < 0.001$, for the 22 CU participants from the same cohort. This shows that the computation of the surface area of putative retinal gliosis was repeatable independent of clinical AD staging. For all the participants from the UAB ADRC, there was no significant difference between the surface area of putative retinal gliosis measured in session 1 (0.80 ± 0.73) versus session 2 (0.81 ± 0.79), $t_{(64)} = -0.163$, $P = 0.87$. The 95% limits of agreement ranged from −0.98 to 0.96 with a mean of the differences of −0.01 (Fig. 3). There was no proportional bias in the Bland-Altman plot, as determined from a linear regression of the differences between the two sessions versus the average, $F_{(1, 63)} = 1.04$, $P = 0.31$ (see Fig. 3). First intra-session gliosis results are reported in subsequent analysis.

Comparison of Putative Retinal Gliosis Between Preclinical AD and Controls

The surface area of putative retinal gliosis was significantly greater in the preclinical AD group (0.97 ± 0.55 mm^2, range = 0.134-2.39, 95% CI for mean = 0.793-1.15, SEM = 0.087) compared to the controls (0.68 ± 0.40 mm^2, range = 0.145-1.36, 95% CI for mean = 0.533-0.821, SEM =0.07); $F_{(1, 70)} = 4.41$, $P = 0.039$, Cohen's d = 0.61 (Fig. 4). Figure 5 represents an example of a larger surface area of putative retinal gliosis in a preclinical AD participant compared to a similarly aged and sex-matched control.

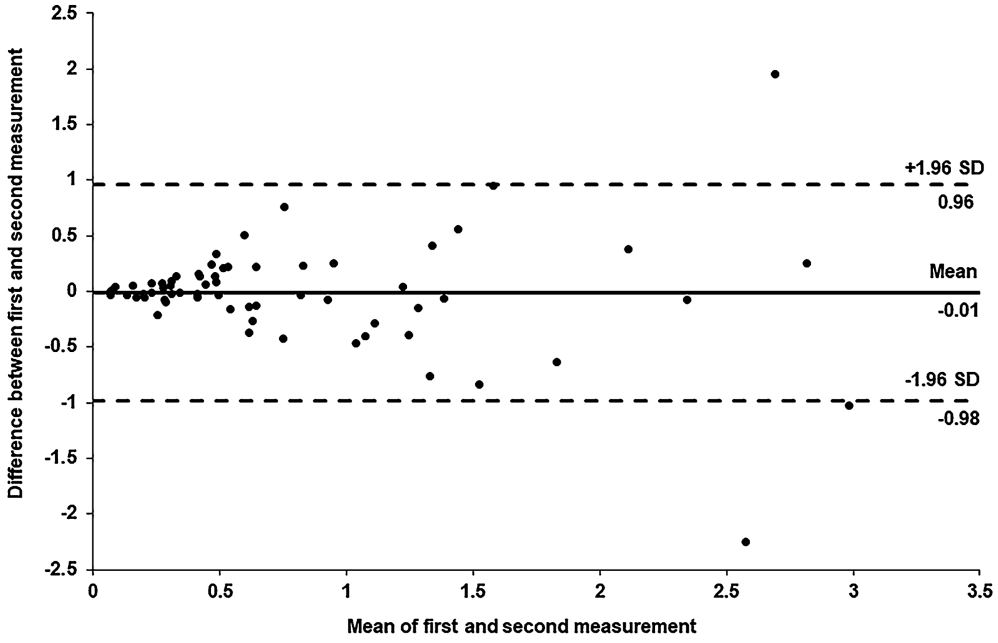

Figure 3. A Bland-Altman plot of the difference between the first and second measurements of putative retinal gliosis from intrasession optical coherence tomography (OCT) images as a function of the mean of two measurements. The *solid line* represents the mean difference between the two measurements and the *dashed lines above* and *below* the mean difference line represents the 95% limits of agreement calculated from the mean and SD of the differences (mean + 1.96*standard deviation = upper limit; mean – 1.96*standard deviation = lower limit). Most data points are within the 95% limits of agreement.

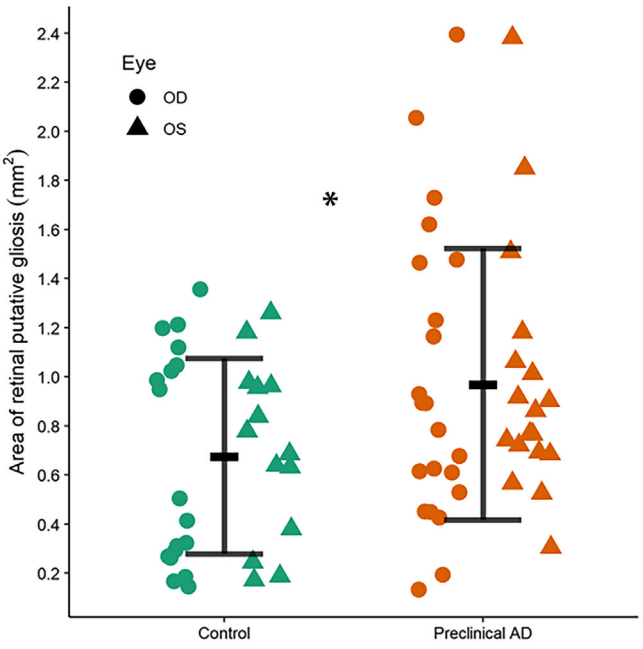

Figure 4. Mean surface area of putative retinal gliosis with standard deviation error bars and individual data points by the eyes in preclinical AD and controls. The surface area of putative retinal gliosis is significantly greater in the preclinical AD group compared to controls ($P = 0.039$) with a moderate effect size (Cohen's d = 0.61). *$P < 0.05$.

Comparison of RNFL Thickness Between Preclinical AD and Controls

RNFL thickness at the nine ETDRS sectors for preclinical AD and controls are summarized in Table 2. There was no statistically significant difference between preclinical AD and controls in terms of RNFL thickness at the nine ETDRS sectors, $P > 0.05$ (see Table 2, Fig. 6). However, there was a trend toward thicker RNFL for the preclinical AD group compared to controls except at the inner temporal region (see Table 2, Fig. 6).

Association Between Surface Area of Putative Retinal Gliosis and RNFL Thickness

Overall, there was a main effect between RNFL thickness and surface area of putative retinal gliosis with the hierarchical model where mean RNFL thickness increases by 1.08 µm per mm^2 increase in the surface area of putative retinal gliosis (t = 2.9, $P = 0.006$). Evaluating the random effects, this was driven much more by regions than subject-level variation. Hence, region level associations were investigated (Tables 3, 4). For the Pearson correlations which do not consider multiplicity/correlations between eyes, there were no significant associations between the surface area of putative retinal gliosis versus central RNFL, inner temporal RNFL, and outer inferior RNFL thickness (see Table 3). However, significant positive correlations were found between the surface area of putative retinal gliosis and inner nasal, outer nasal, inner superior, outer superior, outer temporal and inner inferior RNFL thickness (see Table 3).

Similar patterns/trends in association were observed in the mixed-model variation of the single Pearson correlations in Table 3, although accounting for the eye as

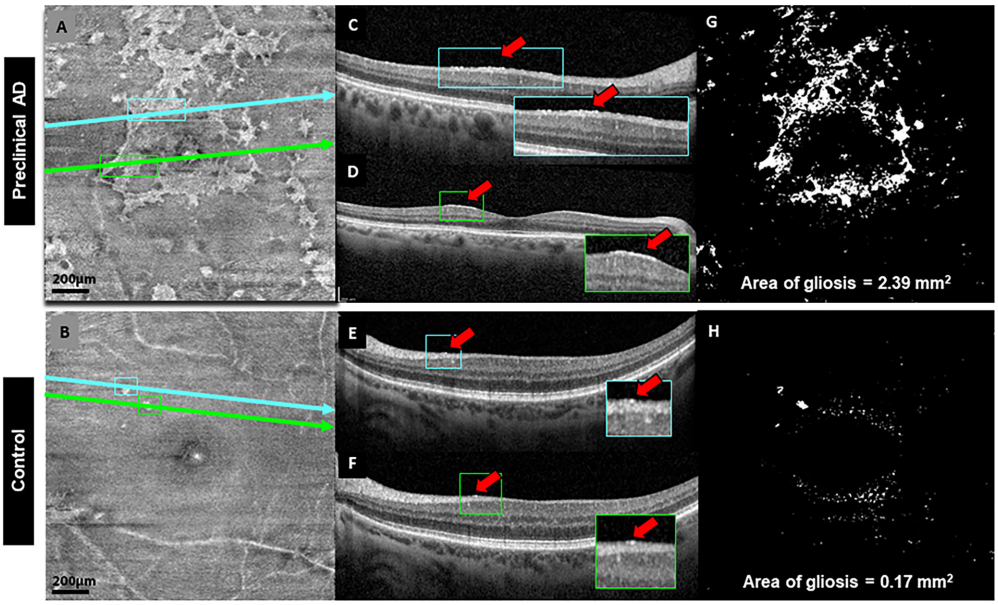

Figure 5. Example of greater surface area of putative retinal gliosis in a 66-year-old female patient with preclinical AD with Aβ PET SUVr of 1.45 (*top panel*) compared to a 68-year-old female control participant with Aβ PET SUVr of 1.09 (*bottom panel*) both with no visible posterior vitreous detachment and history of diabetes. Raw en face MLC slabs depicting increased white or hyper-reflective patchy structures (putative retinal gliosis) in preclinical AD (**A**) compared to the control (**B**). OCT b-scans corresponding to the cross-sectional location of the *blue line* (**C**) and the *green line* (**D**) on (**A**) for preclinical AD and b-scans corresponding to the cross-sectional location of the *blue line* (**E**) and the *green line* (**F**) on (**B**) for the control participant. Hyper-reflective patches representing gliosis on en face MLC slabs (*blue* and *green boxes*) displaying similar color-coded aligned regions of hyper-reflective lines (*red arrows*) on OCT b-scans. Processed images demonstrating larger surface area of putative retinal gliosis in preclinical AD (**G**; surface area of putative retinal gliosis = 2.39 mm^2) versus control (**H**; surface area of putative retinal gliosis = 0.17 mm^2). Scale bar = 200 µm.

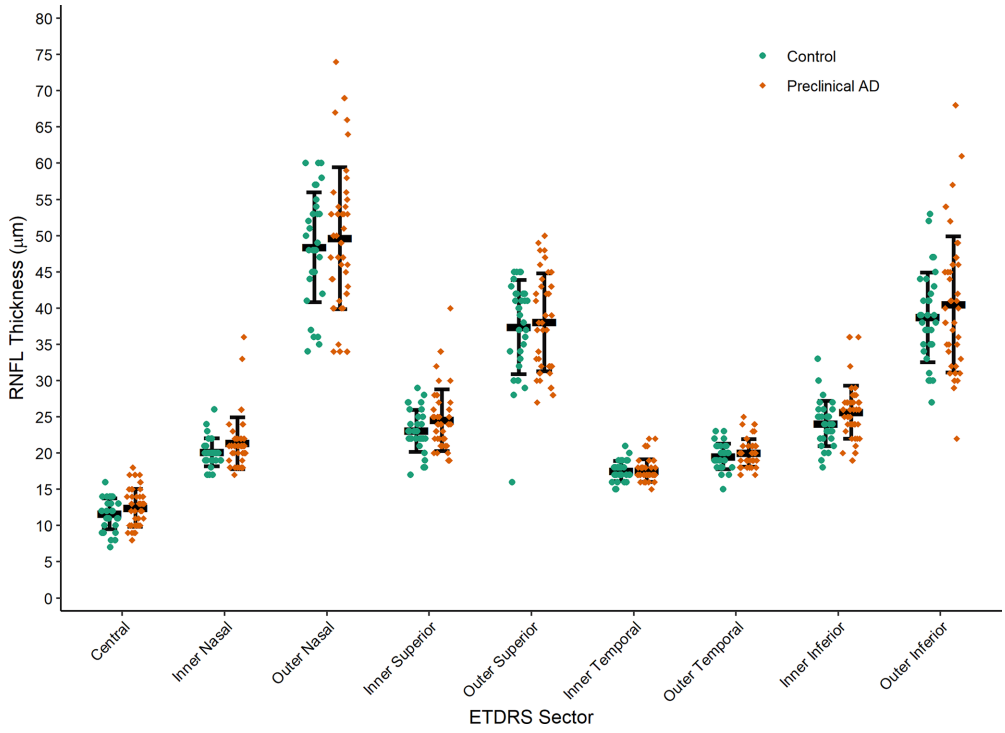

Figure 6. Mean macular retinal nerve fiber layer (mRNFL) thickness with standard deviation error bars and individual data points for the nine sectors of the Early Treatment Diabetic Retinopathy (ETDRS) map. The preclinical AD group did not significantly differ from the control group in mRNFL thickness for all the nine sectors ($P > 0.05$). A trend toward greater mRNFL thickness is observed for all the sectors in the preclinical AD group except at the inner temporal region.

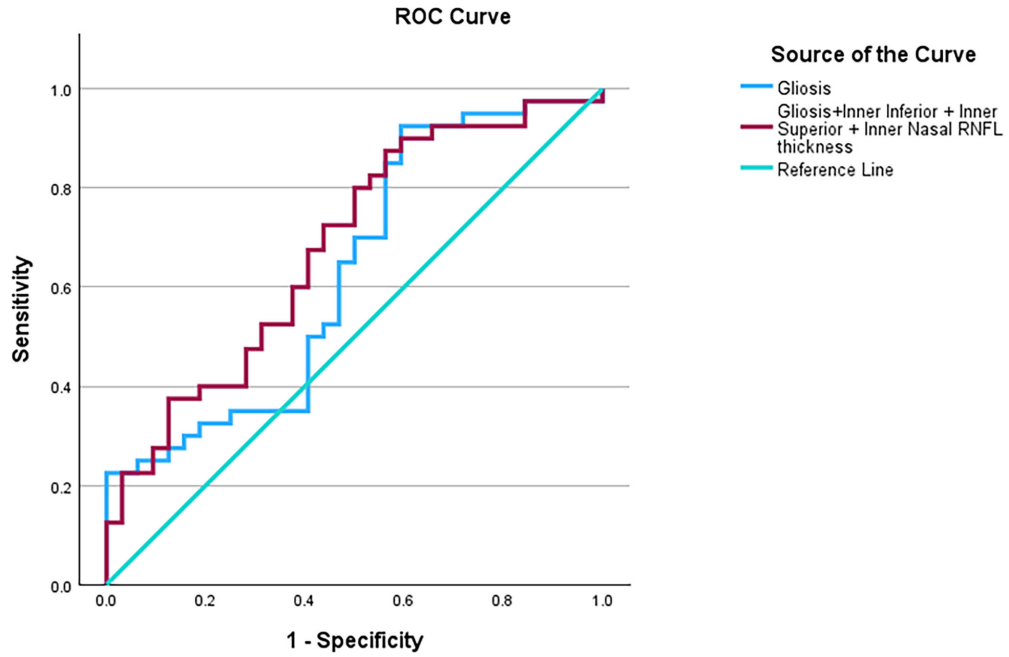

Figure 7. A receiver operating characteristic (ROC) curve showing a model of gliosis and a multimodal model of gliosis, inner inferior, inner superior, and inner nasal RNFL thickness to distinguish between preclinical AD and controls. The ROC model including only gliosis approached significance, AUC = 0.63 (95% CI = 0.50–0.76), $P = 0.05$. The multimodal model which combined the gliosis, inner inferior, inner superior, and inner nasal RNFL thickness yielded a better model which was statistically significant, AUC = 0.68 (95% CI = 0.56–0.81), $P = 0.004$.

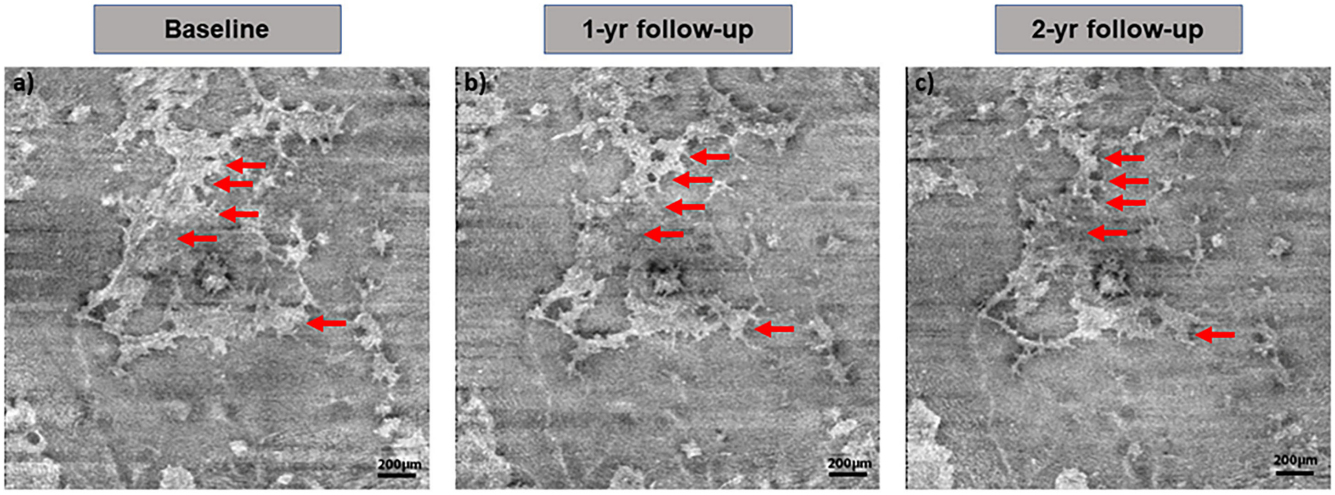

Figure 8. Baseline, 1- and 2-year follow-up images of a 66-year-old female participant with preclinical AD with Aβ PET SUVr of 1.45. The surface area of putative retinal gliosis at baseline (2.39 mm^2; **A**) reduced at 1-year follow-up (1.16 mm^2; **B**), and to a greater extent at the 2-year follow-up (0.96 mm^2; **C**). The *red arrows* show areas of putative retinal gliosis which are reduced at 1- and 2-year follow-ups.

a repeated/within-subject measure did temper the results (see Table 4). Significant positive correlations were found between the surface area of putative retinal gliosis and inner superior, outer temporal, and inner inferior RNFL thickness (see Table 4). Central and inner temporal RNFL thickness were clearly the least associated with the surface area of putative retinal gliosis in both models of associations (see Tables 3, 4). In both models, regions that were thinner generally had weaker associations with the surface area of putative retinal gliosis, especially when considered in the context of thicker regions (see Tables 2–4).

ROC Model of Putative Retinal Gliosis to Distinguish Between Preclinical AD and Controls

The ROC model based on the surface area of putative retinal gliosis alone to distinguish between preclinical AD and controls had a satisfactory AUC of 0.63 (95% CI = 0.50 – 0.76) and approached significance ($P = 0.05$; Fig. 7). A Youden's index of 0.331 was chosen to create a cutoff value of ≥ 0.42 mm^2 for the preclinical AD positive state with a sensitivity of 92.5% and a specificity of 40.6% (see Fig. 7; see Supplementary Fig. S1).

Multimodal ROC Model of Putative Retinal Gliosis and RNFL Thickness to Distinguish Between Preclinical AD and Controls

Interestingly, an ROC model which combined the surface area of putative retinal gliosis, inner inferior, inner superior, and inner nasal RNFL thickness to distinguish between preclinical AD and controls yielded a modestly better model which was statistically significant, AUC = 0.68 (95% CI = 0.56 – 0.81), $P = 0.004$ (see Fig. 7). A Youden's index of 0.313 was chosen to create a cutoff predictive value of ≥ 0.43. The cutoff predictive value corresponded to a gliosis surface area of ≥ 0.45 mm^2, inner inferior RNFL thickness of ≥ 24 µm, inner superior RNFL thickness of ≥ 21 µm, and inner nasal RNFL thickness of ≥ 20 µm for the preclinical AD positive state with a sensitivity of 87.5% and a specificity of 43.8% (see Fig. 7, see Supplementary Fig. S1).

Case-in-Point Example of a Longitudinal Change in Putative Retinal Gliosis in Preclinical AD

Figure 8 shows a baseline, 1-, and 2-year follow-up images of a 66-year-old female preclinical AD participant with Aβ PET SUVr of 1.45. The surface area of putative retinal gliosis at baseline (2.39 mm^2; see Fig. 8A) reduced at 1-year follow-up (1.16 mm^2; see Fig. 8B), and to a greater extent at the 2-year follow-up (0.96 mm^2; see Fig. 8C).

Discussion

One of the major findings of the study is the larger surface area of putative retinal gliosis in preclinical AD compared to similarly aged controls with a moderate effect size. However, no significant differences in the mRNFL thickness in the nine ETDRS sectors were observed between the two groups. Nevertheless, there was a trend toward thicker RNFL in the preclinical AD group compared to controls. Significant positive associations were found between the surface area of putative retinal gliosis and global RNFL thickness as well as at specific sectors, suggesting a possible contribution of gliosis to RNFL thickening. Whereas a borderline significant ROC model using surface area of putative retinal gliosis alone was obtained for distinguishing preclinical AD from controls, a combined model considering the surface area of putative retinal gliosis alongside specific RNFL thicknesses showed improved specificity which was significant. In addition, gliosis computations were found to be a reliable measure of AD-related neuroinflammation to allow for early disease detection. Last, a case-in-point longitudinal change of putative retinal gliosis was shown in a preclinical AD participant, suggesting the possible use of putative retinal gliosis to monitor disease progression.

Increased gliosis or immunoreactivity in AD has been mostly studied ex vivo or through animal models. Broadly, elevated levels of inflammatory markers and risk genes linked to immune system function in individuals with AD have highlighted the role of neuroinflammation in the early pathogenesis of AD (preclinical AD).[71–73] The co-existence of reactive immune cells with Aβ plaques further emphasizes the critical role that neuroinflammation plays in the amyloid pathological cascade of AD.[74] Specifically, astrocyte dysfunction and microglial activation have been noted to commence during the presymptomatic stages (preclinical AD), stabilizing/declining as the disease progresses from early to late stages of MCI and prior to neurodegeneration in the dementia stage of the disease.[75] Thus, neuroinflammation occurs in preclinical AD prior to neurodegeneration in the dementia stage of the disease. In agreement with brain histological studies, the retina viewed as an extension of the brain, also exhibits the implication of neuroinflammation in retinal counterparts like the Müller cells, astrocytes, and microglia. Mouse models of AD and postmortem biopsy of patients with AD have revealed retinal glial activation analogous to the CNS immunoreactivity.[26–28] In addition, larger area of hyper-reflective granular membranes hypothesized as manifestations of inner retinal gliosis has been shown in individuals with early cognitive impairment due to AD compared to controls on high-resolution in vivo imaging, such as AO scanning laser ophthalmoscopy (AOSLO).[76] Our finding of larger surface area of putative retinal gliosis in preclinical AD compared to controls via en face SD-OCT in vivo imaging is consistent with findings of increased neuroinflammation in mouse models of AD and postmortem biopsy of patients with AD, as well as those found on advanced in vivo imaging such as AOSLO.[26–28,76] The moderate effect size found for the surface of putative retinal gliosis in preclinical AD suggests a possible clinical usability of this metric for early detection of the disease.

In the retinal histopathological study by Xu et al., higher microgliosis was found in the mid-peripheral retina of AD donor eyes compared to controls.[26] Interestingly, these mid-peripheral regions of microgliosis co-localized with Aβ deposits in both the AD and control donor eyes.[26] These findings propose a possible mechanism triggering neuroinflammation subsequent to the initial deposition of Aβ in the AD retina. Similar investigations can be done via a multimodal in vivo imaging model involving Blue Autofluorescence imaging[34,77] and en face SD-OCT to determine whether areas of putative retinal gliosis are co-localized with retinal amyloid/inclusion bodies when the two images are overlapped. This will be done in future studies as the next progression of the current study. Furthermore, various studies have reported a decline or stabilization in heightened gliosis from early (preclinical AD) to later stages of AD,[75,78] suggesting neuroinflammation (in early disease) precedes neurodegeneration (in later disease) in AD. This assessment is consistent with our case-in-point example of a longitudinal change in preclinical AD where the surface area of putative retinal gliosis reduced in follow-up visits compared to baseline. This finding in addition to our cross-sectional results of higher putative retinal gliosis in preclinical AD provides the foundation for a larger longitudinal study to investigate the use of the surface area of putative retinal gliosis to monitor disease progression in preclinical AD.

The retina comprises of two primary glial cell types: macroglia, which include astrocytes and Müller cells, and microglia. Müller cells are the predominant glial cells of the retina traversing the entire neurosensory retina.[79] Astrocytes are stellate glial cells mostly found in the RNFL in close association with blood vessels.[40] Microglial cells are largely present in the IPL and OPL, but a smaller portion are also found in the RGC, RNFL, and at the ILM.[39] During gliosis, these glial cells become activated and undergo alterations in their structure and behavior. They might proliferate, change their shape, and release signaling molecules, cytokines, or other factors in response to the presence of pathogens or injury. Observations of heightened retinal hyper-reflectivity at the ILM-RNFL junction speculated as putative retinal gliosis in our study aligns with the convergence of astrocytes,

Investigative Ophthalmology & Visual Science

Müller cells' end feet, and microglia. Given this anatomic convergence, the macrophages depicted in the MLC en face slabs of our study might represent a collective activation of all three glial cell types. It is also appropriate to hypothesize that the observed retinal changes might be linked to astrogliosis, particularly considering the proximity of the hyper-reflectivity to the vessels (see Figs. 1, 5). However, hyper-reflectivity in areas not adjacent to the vessels could denote microglial activation contributing to the retinal inflammation (see Figs. 1, 5). Another study argues that these could possibly be vitreous hyalocytes rather than retinal microglia even though this study used an en face slab located above the ILM.[80] Deciphering the distinct types of glial activation during the early stages of the disease will be crucial for understanding disease mechanisms and devising targeted therapeutic approaches. This could be done via advanced high-resolution in vivo imaging, such as AO-OCT, as has been done in multiple sclerosis,[81] or a combination of histology and high-resolution in vivo imaging.

RNFL thickness in the macular region showed no significant difference in the nine ETDRS sectors between the two groups. This finding is comparable to other studies that reported no significant differences in the RNFL thickness in preclinical AD.[32–34] The lack of significance in RNFL thickness between the two groups could be due to the fact that the entire hyper-reflective band of the RNFL on SD-OCT is not made up only RNFL bundles but contains non-neural components including glial and blood vessels.[39–43] Variability in blood vessel diameter and the non-neural components may cause artifacts in thickness measurements and, in turn, mask an assessment of subtle changes in the RNFL bundle in preclinical AD. Interestingly, there was a trend toward greater RNFL thickness in the preclinical AD group compared to controls in all sectors except at the inner temporal region. There were significant positive associations between the surface area of putative retinal gliosis and RNFL thickness globally, and at specific retinal sectors with areas of thicker retinas having a stronger association with putative retinal gliosis and vice versa. These associations suggest that the trend toward thicker RNFL in the preclinical AD group could be due to the presence of putative gliosis in the RNFL hyper-reflective band. This assessment is consistent with prior studies that hypothesized that thicker mRNFL in MCI due to AD may be due of neuroinflammation.[21,31] However, we provide actual quantitative data of putative retinal gliosis in our study to show this association compared to prior studies.[21,31]

Gliosis was least associated with central and inner temporal RNFL thickness in both models of association. This could be due to the absence/decreased retinal nerve fibers at those locations. The central region of the macular does not contain retinal nerve fibers, and the inner temporal region is made up of low-density temporal raphe[45,46] which could contribute to these nonsignificant correlations. Putative retinal gliosis measurements were of good reliability independent of clinical AD staging. This shows that the surface area of putative retinal gliosis is a reliable measure of AD-related neuroinflammation to be used for early detection of AD.

A single retinal biomarker may not be sensitive or specific to AD because the biomarker may be indicated in other retinal diseases. For example, putative retinal gliosis has been indicated in glaucoma,[45,48–50] diabetic retinopathy,[51–53] retinal vein occlusion,[54] and ERM.[63] Even though these conditions were clinically excluded from our study, it may explain the reason why the multimodal model of putative retinal gliosis and RNFL thickness yielded a better AUC and specificity compared to the unimodal of putative retinal gliosis alone. Thus, preclinical manifestations of the above retinal conditions may be difficult to distinguish from putative retinal gliosis in preclinical AD. Although a retinal structural metric such as the surface area of putative retinal gliosis may have advantages over other known structural metrics (RNFL thickness), it currently appears that the way forward as a field is to utilize a multimodal approach that combines both structural metrics to improve the AUC and specificity of these metrics for early AD detection. Our results of a better multimodal model distinguishing between preclinical AD and controls are consistent with findings of our previous study that investigated a multimodal model of the mid-peripheral capillary free zones and other vascular metrics for early AD risk detection.[17] It is also consistent with results of a previous study that investigated a multimodal model of fractal and lacunarity analysis to distinguish between cognitively impaired and CU older adults.[82]

Blood-based biomarkers are currently at the forefront of scientific exploration, showcasing tremendous growth. However, most blood-based biomarkers do not do well in early AD probably due to the fact that, unlike the retina, which is a direct extension of the brain, blood-based biomarkers are derived via a downstream effect from the CNS and can be influenced by genetic factors and renal function.[17] Elevated levels of glial fibrillary acidic protein (GFAP), an astrocytic protein signifying astrogliosis, have been identified in blood samples and linked to preclinical AD.[12] Additionally, plasma levels of Aβ42/Aβ40 ratio and p-tau 217 are elevated in individuals with preclinical AD.[13,14] This surge in research focusing on blood-based biomarkers prompts our immediate attention to compare and evaluate their association with putative retinal gliosis. Given the flourishing trend in blood-based biomarker research within neurodegenerative diseases, another crucial future direction for this study involves examining a combined model of putative retinal gliosis and blood-based biomarkers (GFAP, Aβ42/Aβ40 ratio, and p-tau 217) to improve the sensitivity, and specificity of both biomarkers for preclinical AD detection.

The limitations of the study include its cross-sectional nature. However, our cross-sectional results of larger surface area of putative retinal gliosis in preclinical AD as well as the case-in-point example of a longitudinal change in putative retinal gliosis sets up the foundation for a larger longitudinal study to investigate the use of this metric for monitoring disease progression in preclinical AD. In addition, en face SD-OCT imaging does not have the lateral resolution to resolve the types of glial cells in these areas of presumed gliosis. Future studies should focus on histology and high-resolution in vivo imaging such as AO-OCT to resolve these cells. The MATLAB software used in the computation of the surface area of putative retinal gliosis also needs to be made available on commercial SD-OCT devices. It is imperative to mention that en face imaging modality is present in most current commercial OCT systems, making its incorporation as a screening tool for AD feasible in eye care practices or community health settings. We used a 20 × 20 degrees dense scan solely for the purpose of generating en face images and 30 × 25 degrees scan for RNFL thickness measurements using the ETDRS grid. En face images cannot be generated from the 30 × 25 degrees scan because of its coarse nature. However, the scan is large enough to encompass the entire area of the ETDRS grid compared to the dense

Investigative Ophthalmology & Visual Science

20 × 20 degrees scan where portions of the ETDRS grid (outer superior, inferior, nasal, and temporal regions) are not adequately accounted for. We therefore chose the larger field of view of the 30 × 25 degrees scan to compute the RNFL thickness, even though it has less sampling compared to the 20 × 20 degrees scan. It is also important to mention that we have previously published our protocol for mRNFL thickness measurement,[66] and the current work is an extension of our previous publication.

In conclusion, our analysis showed greater putative retinal gliosis in preclinical AD compared to similarly aged controls with a moderate effect size. This suggests putative retinal gliosis as a potential biomarker for AD-related neuroinflammation. A multimodal analysis of putative retinal gliosis and RNFL thickness yielded a better AUC and specificity compared to gliosis alone for preclinical AD detection. This finding indicates that a multimodal retinal structural approach would be more valuable for early AD detection to utilize in future research going forward. Our analysis shows that RNFL thickening could be explained by putative retinal gliosis. These findings suggest the potential value of the surface area of putative retinal gliosis in early AD detection, monitoring disease progression, and serving as surrogate end points for neuroinflammation in clinical trials related to AD.

Acknowledgments

The authors wish to thank participants from the UAB ADRC and ARIAS who were extremely generous with their time for this study to help advance research into the early detection of AD.

Supported by NIH/NIA R21AG079794 to E.A., NIH/NIA P20AG068024 to E.D.R., and part of the Atlas of Retinal Imaging in Alzheimer's Study (ARIAS) supported by a generous grant from the Morton Plant Mease Health Care Foundation (Clearwater, FL, USA) to P.J.S. and Stuart Sinoff (co-principal investigators).

Disclosure: **S. Ravichandran**, None; **P.J. Snyder**, None; **J. Alber**, None; **M.R. Kenny**, None; **A. Rothstein**, None; **K. Brown**, None; **C.F. Murchison**, None; **O.J. Clay**, None; **E.D. Roberson**, None; **E. Arthur**, None

References

1. 2023 Alzheimer's disease facts and figures. *Alzheimers Dement*. 2023;19(4):1598–1695.
2. La Rue A, Jarvik LF. Cognitive function and prediction of dementia in old age. *Int J Aging Hum Dev*. 1987;25(2):79–89.
3. Linn RT, Wolf PA, Bachman DL, et al. The 'preclinical phase' of probable Alzheimer's disease. A 13-year prospective study of the Framingham cohort. *Arch Neurol*. 1995;52(5):485–490.
4. Braak H, Braak E. Frequency of stages of Alzheimer-related lesions in different age categories. *Neurobiol Aging*. 1997;18(4):351–357.
5. Snowdon DA, Kemper SJ, Mortimer JA, Greiner LH, Wekstein DR, Markesbery WR. Linguistic ability in early life and cognitive function and Alzheimer's disease in late life. Findings from the Nun Study. *JAMA*. 1996;275(7):528–532.
6. Elias MF, Beiser A, Wolf PA, Au R, White RF, D'Agostino RB. The preclinical phase of Alzheimer disease: a 22-year prospective study of the Framingham Cohort. *Arch Neurol*. 2000;57(6):808–813.
7. Gordon BA, Blazey TM, Su Y, et al. Spatial patterns of neuroimaging biomarker change in individuals from families with autosomal dominant Alzheimer's disease: a longitudinal study. *Lancet Neurol*. 2018;17(3):241–250.
8. Sperling RA, Aisen PS, Beckett LA, et al. Toward defining the preclinical stages of Alzheimer's disease: recommendations from the National Institute on Aging-Alzheimer's Association workgroups on diagnostic guidelines for Alzheimer's disease. *Alzheimers Dement*. 2011;7(3):280–292.
9. Jack CR, Jr, Albert MS, Knopman DS, et al. Introduction to the recommendations from the National Institute on Aging-Alzheimer's Association workgroups on diagnostic guidelines for Alzheimer's disease. *Alzheimers Dement*. 2011;7(3):257–262.
10. Jack CR, Jr, Bennett DA, Blennow K, et al. NIA-AA Research Framework: toward a biological definition of Alzheimer's disease. *Alzheimers Dement*. 2018;14(4):535–562.
11. Sperling RA, Donohue MC, Raman R, et al. Association of factors with elevated amyloid burden in clinically normal older individuals. *JAMA Neurol*. 2020;77(6):735–745.
12. Chatterjee P, Pedrini S, Stoops E, et al. Plasma glial fibrillary acidic protein is elevated in cognitively normal older adults at risk of Alzheimer's disease. *Transl Psychiatry*. 2021;11(1):27.
13. Fandos N, Pérez-Grijalba V, Pesini P, et al. Plasma amyloid β 42/40 ratios as biomarkers for amyloid β cerebral deposition in cognitively normal individuals. *Alzheimers Dement (Amst)*. 2017;8:179–187.
14. Jonaitis EM, Janelidze S, Cody KA, et al. Plasma phosphorylated tau 217 in preclinical Alzheimer's disease. *Brain Commun*. 2023;5(2):fcad057.
15. London A, Benhar I, Schwartz M. The retina as a window to the brain-from eye research to CNS disorders. *Nat Rev Neurol*. 2013;9(1):44–53.
16. Chiquita S, Rodrigues-Neves AC, Baptista FI, et al. The retina as a window or mirror of the brain changes detected in Alzheimer's disease: critical aspects to unravel. *Mol Neurobiol*. 2019;56(8):5416–5435.
17. Arthur E, Ravichandran S, Snyder PJ, et al. Retinal mid-peripheral capillary free zones are enlarged in cognitively unimpaired older adults at high risk for Alzheimer's disease. *Alzheimers Res Ther*. 2023;15(1):172.
18. Salobrar-Garcia E, Hoyas I, Leal M, et al. Analysis of retinal peripapillary segmentation in early Alzheimer's disease patients. *Biomed Res Int*. 2015;2015:636548.
19. Gao L, Liu Y, Li X, Bai Q, Liu P. Abnormal retinal nerve fiber layer thickness and macula lutea in patients with mild cognitive impairment and Alzheimer's disease. *Arch Gerontol Geriatr*. 2015;60(1):162–167.
20. Coppola G, Di Renzo A, Ziccardi L, et al. Optical coherence tomography in Alzheimer's disease: a meta-analysis. *PLoS One*. 2015;10(8):e0134750.
21. Ascaso FJ, Cruz N, Modrego PJ, et al. Retinal alterations in mild cognitive impairment and Alzheimer's disease: an optical coherence tomography study. *J Neurol*. 2014;261(8):1522–1530.
22. den Haan J, Verbraak FD, Visser PJ, Bouwman FH. Retinal thickness in Alzheimer's disease: a systematic review and meta-analysis. *Alzheimers Dement (Amst)*. 2017;6:162–170.
23. Chan VTT, Sun Z, Tang S, et al. Spectral-domain oct measurements in Alzheimer's disease: a systematic review and meta-analysis. *Ophthalmology*. 2019;126(4):497–510.
24. Lyman M, Lloyd DG, Ji X, Vizcaychipi MP, Ma D. Neuroinflammation: the role and consequences. *Neurosci Res*. 2014;79:1–12.
25. Calsolaro V, Edison P. Neuroinflammation in Alzheimer's disease: current evidence and future directions. *Alzheimers Dement*. 2016;12(6):719–732.

26. Xu QA, Boerkoel P, Hirsch-Reinshagen V, et al. Müller cell degeneration and microglial dysfunction in the Alzheimer's retina. *Acta Neuropathol Commun*. 2022;10:145.
27. Grimaldi A, Brighi C, Peruzzi G, et al. Inflammation, neurodegeneration and protein aggregation in the retina as ocular biomarkers for Alzheimer's disease in the 3xTg-AD mouse model. *Cell Death Dis*. 2018;9:685.
28. Edwards MM, Rodríguez JJ, Gutierrez-Lanza R, Yates J, Verkhratsky A, Lutty GA. Retinal macroglia changes in a triple transgenic mouse model of Alzheimer's disease. *Exp Eye Res*. 2014;127:252–260.
29. Langmann T. Microglia activation in retinal degeneration. *J Leukoc Biol*. 2007;81(6):1345–1351.
30. Karlstetter M, Scholz R, Rutar M, Wong WT, Provis JM, Langmann T. Retinal microglia: just bystander or target for therapy?. *Prog Retin Eye Res*. 2015;45:30–57.
31. Lad EM, Mukherjee D, Stinnett SS, et al. Evaluation of inner retinal layers as biomarkers in mild cognitive impairment to moderate Alzheimer's disease. *PLoS One*. 2018;13(2):e0192646.
32. van de Kreeke JA, Nguyen HT, den Haan J, et al. Retinal layer thickness in preclinical Alzheimer's disease. *Acta Ophthalmol*. 2019;97(8):798–804.
33. Golzan SM, Goozee K, Georgevsky D, et al. Retinal vascular and structural changes are associated with amyloid burden in the elderly: ophthalmic biomarkers of preclinical Alzheimer's disease. *Alzheimers Res Ther*. 2017;9(1):13.
34. Snyder PJ, Johnson LN, Lim YY, et al. Nonvascular retinal imaging markers of preclinical Alzheimer's disease. *Alzheimers Dement (Amst)*. 2016;4:169–178.
35. Paquet C, Boissonnot M, Roger F, Dighiero P, Gil R, Hugon J. Abnormal retinal thickness in patients with mild cognitive impairment and Alzheimer's disease. *Neurosci Lett*. 2007;420(2):97–99.
36. Kesler A, Vakhapova V, Korczyn AD, Naftaliev E, Neudorfer M. Retinal thickness in patients with mild cognitive impairment and Alzheimer's disease. *Clin Neurol Neurosurg*. 2011;113(7):523–526.
37. Shen Y, Liu L, Cheng Y, et al. Retinal nerve fiber layer thickness is associated with episodic memory deficit in mild cognitive impairment patients. *Curr Alzheimer Res*. 2014;11(3):259–266.
38. Knoll B, Simonett J, Volpe NJ, et al. Retinal nerve fiber layer thickness in amnestic mild cognitive impairment: case-control study and meta-analysis. *Alzheimers Dement (Amst)*. 2016;4:85–93.
39. Rathnasamy G, Foulds WS, Ling EA, Kaur C. Retinal microglia - a key player in healthy and diseased retina. *Prog Neurobiol*. 2019;173:18–40.
40. Vecino E, Rodriguez FD, Ruzafa N, Pereiro X, Sharma SC. Glia-neuron interactions in the mammalian retina. *Prog Retin Eye Res*. 2016;51:1–40.
41. Au NPB, Ma CHE. Neuroinflammation, microglia and implications for retinal ganglion cell survival and axon regeneration in traumatic optic neuropathy. *Front Immunol*. 2022;13:860070.
42. Büssow H. The astrocytes in the retina and optic nerve head of mammals: a special glia for the ganglion cell axons. *Cell Tissue Res*. 1980;206(3):367–378.
43. Ogden TE. Nerve fiber layer of the primate retina: thickness and glial content. *Vision Res*. 1983;23(6):581–587.
44. Hood DC, Fortune B, Mavrommatis MA, et al. Details of glaucomatous damage are better seen on OCT en face images than on OCT retinal nerve fiber layer thickness maps. *Invest Ophthalmol Vis Sci*. 2015;56(11):6208–6216.
45. Ashimatey BS, King BJ, Swanson WH. Retinal putative glial alterations: implication for glaucoma care. *Ophthalmic Physiol Opt*. 2018;38(1):56–65.
46. Ashimatey BS, King BJ, Burns SA, Swanson WH. Evaluating glaucomatous abnormality in peripapillary optical coherence tomography enface visualisation of the retinal nerve fibre layer reflectance. *Ophthalmic Physiol Opt*. 2018;38(4):376–388.
47. Arthur E, Papay JA, Haggerty BP, Clark CA, Elsner AE. Subtle changes in diabetic retinas localised in 3D using OCT. *Ophthalmic Physiol Opt*. 2018;38(5):477–491.
48. Grieshaber MC, Orgul S, Schoetzau A, Flammer J. Relationship between retinal glial cell activation in glaucoma and vascular dysregulation. *J Glaucoma*. 2007;16(2):215–219.
49. Grieshaber MC, Moramarco F, Schoetzau A, Flammer J, Orguel S. Detection of retinal glial cell activation in glaucoma by time domain optical coherence tomography. *Klin Monbl Augenheilkd*. 2012;229(4):314–318.
50. Cheung H, King BJ, Gast TJ. Presumed activated retinal astrocytes and Müller cells in healthy and glaucomatous eyes detected by spectral domain optical coherence tomography. *Ophthalmic Physiol Opt*. 2020;40(6):738–751.
51. Ong JX, Nesper PL, Fawzi AA, Wang JM, Lavine JA. Macrophage-like cell density is increased in proliferative diabetic retinopathy characterized by optical coherence tomography angiography. *Invest Ophthalmol Vis Sci*. 2021;62(10):2.
52. Zhang NT, Nesper PL, Ong JX, Wang JM, Fawzi AA, Lavine JA. Macrophage-like cells are increased in patients with vision-threatening diabetic retinopathy and correlate with macular edema. *Diagnostics (Basel)*. 2022;12(11):2793.
53. Wang W, Sun G, Xu A, Chen C. Proliferative diabetic retinopathy and diabetic macular edema are two factors that increase macrophage-like cell density characterized by en face optical coherence tomography. *BMC Ophthalmol*. 2023;23(1):46.
54. Wang W, Sun G, He L, Chen C. Increased macrophage-like cell density in retinal vein occlusion as characterized by en face optical coherence tomography. *J Clin Med*. 2022;11(19):5636.
55. Bennett AG, Rudnicka AR, Edgar DF. Improvements on Littmann's method of determining the size of retinal features by fundus photography. *Graefes Arch Clin Exp Ophthalmol*. 1994;232:361–367.
56. Smith T, Gildeh N, Holmes C. The Montreal Cognitive Assessment: validity and utility in a memory clinic setting. *Can J Psychiatry*. 2007;52(5):329–332.
57. Nasreddine ZS, Phillips NA, Bédirian V, et al. The Montreal Cognitive Assessment, MoCA: a brief screening tool for mild cognitive impairment. *J Am Geriatr Soc*. 2005;53(4):695–699.
58. Hughes CP, Berg L, Danziger W, Coben LA, Martin RL. A new clinical scale for the staging of dementia. *Br J Psychiatry*. 1982;140(6):566–572.
59. Karantzoulis S, Novitski J, Gold M, Randolph C. The repeatable battery for the assessment of neuropsychological status (RBANS): utility in detection and characterization of mild cognitive impairment due to Alzheimer's disease. *Arch Clin Neuropsychol*. 2013;28(8):837–844.
60. Randolph C, Tierney MC, Mohr E, Chase TN. The repeatable battery for the assessment of neuropsychological status (RBANS): preliminary clinical validity. *J Clin Exp Neuropsychol*. 1998;20(3):310–319.
61. Faul F, Erdfelder E, Buchner A, Lang AG. Statistical power analyses using G*Power 3.1: tests for correlation and regression analyses. *Behav Res Methods*. 2009;41(4):1149–1160.
62. Jia Y, Tan O, Tokayer J, et al. Split-spectrum amplitude-decorrelation angiography with optical coherence tomography. *Opt Express*. 2012;20(4):4710–4725.
63. Grondin C, Au A, Wang D, et al. Identification and characterization of epivascular glia using en face optical coherence tomography. *Am J Ophthalmol* 2021;229:108–119.

Investigative Ophthalmology & Visual Science

64. Hammer DX, Agrawal A, Villanueva R, Saeedi O, Liu Z. Label-free adaptive optics imaging of human retinal macrophage distribution and dynamics. *Proc Natl Acad Sci U S A*. 2020;117(48):30661–30669.
65. Aboshosha A, Hassan M, Ashour M, El Mashade M. Image denoising based on spatial filters, an analytical study. *International Conference on Computer Engineering & Systems*. 2009:245–250.
66. Alber J, Arthur E, Sinoff S, et al. A recommended "minimum data set" framework for SD-OCT retinal image acquisition and analysis from the Atlas of Retinal Imaging in Alzheimer's Study (ARIAS). *Alzheimers Dement (Amst)*. 2020;12(1):e12119.
67. Early Treatment Diabetic Retinopathy Study Research Group. Grading diabetic retinopathy from stereoscopic color fundus photographs–an extension of the modified Airlie House classification. ETDRS report number 10. *Ophthalmology*. 1991;98(5):786–806.
68. Wong BM, Cheng RW, Mandelcorn ED, et al. Validation of optical coherence tomography retinal segmentation in neurodegenerative disease. *Transl Vis Sci Technol*. 2019;8(5):6.
69. Koo TK, Li MY. A guideline of selecting and reporting intraclass correlation coefficients for reliability research. *J Chiropr Med*. 2016;15(2):155–163.
70. Giavarina D. Understanding Bland Altman analysis. *Biochem Med (Zagreb)*. 2015;25(2):141–151.
71. Leng F, Edison P. Neuroinflammation and microglial activation in Alzheimer disease: where do we go from here?. *Nat Rev Neurol*. 2021;17(3):157–172.
72. Tan ZS, Beiser AS, Vasan RS, et al. Inflammatory markers and the risk of Alzheimer disease: the Framingham Study. *Neurology*. 2007;68(22):1902–1908.
73. Akiyama H, Barger S, Barnum S, et al. Inflammation and Alzheimer's disease. *Neurobiol Aging*. 2000;21(3):383–421.
74. Mandybur TI. Cerebral amyloid angiopathy and astrocytic gliosis in Alzheimer's disease. *Acta Neuropathol*. 1989;78(3):329–331.
75. Bjorkli C, Sandvig A, Sandvig I. Bridging the gap between fluid biomarkers for Alzheimer's disease, model systems, and patients. *Front Aging Neurosci*. 2020;12:272.
76. Zhang YS, Onishi AC, Zhou N, et al. Characterization of inner retinal hyperreflective alterations in early cognitive impairment on adaptive optics scanning laser ophthalmoscopy. *Invest Ophthalmol Vis Sci*. 2019;60(10):3527–3536.
77. Koronyo Y, Biggs D, Barron E, et al. Retinal amyloid pathology and proof-of-concept imaging trial in Alzheimer's disease. *JCI Insight*. 2017;2(16):e93621.
78. Hoozemans JJ, Rozemuller AJ, van Haastert ES, Eikelenboom P, van Gool WA. Neuroinflammation in Alzheimer's disease wanes with age. *J Neuroinflammation*. 2011;8(1):1–8.
79. Reichenbach A, Bringmann A. New functions of Müller cells. *Glia*. 2013;61(5):651–678.
80. Castanos MV, Zhou DB, Linderman RE, et al. Imaging of macrophage-like cells in living human retina using clinical OCT. *Invest Ophthalmol Vis Sci*. 2020;61(6):48.
81. Hammer DX, Kovalick K, Liu Z, Chen C, Saeedi OJ, Harrison DM. Cellular-level visualization of retinal pathology in multiple sclerosis with adaptive optics. *Invest Ophthalmol Vis Sci*. 2023;64(14):21.
82. Cabrera DeBuc D, Feuer WJ, Persad PJ, et al. Investigating vascular complexity and neurogenic alterations in sectoral regions of the retina in patients with cognitive impairment. *Front Physiol*. 2020;11:570412.

Investigative Ophthalmology & Visual Science